

Theory of ion and water transport in reverse osmosis membranes

Y.S. Oren and P.M. Biesheuvel

Wetsus, European Centre of Excellence for Sustainable Water Technology
Oostergoweg 9, 8911 MA Leeuwarden, The Netherlands

Abstract

We present theory for ion and water transport through reverse osmosis membranes based on a Maxwell-Stefan framework combined with hydrodynamic theory for the reduced motion of particles in thin pores. We include all driving forces and frictions both on the fluid (water), and on the ions, including ion-fluid friction as well as ion-wall friction. By including the acid-base character of the carbonic acid system, the boric acid system, $\text{H}_3\text{O}^+/\text{OH}^-$, and the membrane charge, we locally determine pH and thus the effective charge of the membrane as well as the dissociation degree of boric acid. We present calculation results for a “dead end” experiment with fixed feed concentration, where effluent composition is a self-consistent function of fluxes through the membrane. Comparison with experimental results from literature for fluid flow vs. pressure, and for salt and boron rejection, shows that theory agrees well with data. Our model is based on realistic assumptions for the effective sizes of the ions and for the diameter of the RO membrane pore in the polyamide toplayer (~ 0.75 nm).

1 Introduction

In a world where potable water is a scarce natural resource, a need develops to produce it by artificial means [1]. This trend is expected to increase the consumption of desalinated water dramatically over the coming years [2]. Reverse osmosis (RO) has become an increasingly popular solution in many countries to provide potable water. About 98% of Earth’s water is seawater (SW) and brackish water (BW), making these attractive sources.

The principle of RO is to apply high pressure on an aqueous solution which is in contact with a membrane that allows passage of water, but not of salts. If the pressure is high enough to overcome the osmotic pressure of the solution, water will pass the membrane, resulting in a low-in-salts permeate stream. The possibility of desalinating water by the RO principle was already researched in the 1850s [3] but it was not until the 1960s, when cellulose acetate (CA) membranes were introduced, that RO gained real industrial potential for the production of desalinated water. Still, there were many issues to be solved in order to make RO commercially competitive, and ultimately the preferred technology. One of the major issues at that time was the high energy consumption required to operate an RO desalination plant. Since the osmotic pressure of seawater is about thirty bars, the pressure that has to be applied to overcome the osmotic pressure is “lost” with the brine. In the 1980s energy recovery devices for RO were introduced, to recover the potential energy in the brine. Together with the introduction of thin-film composite (TFC) polyamide (PA) membranes that increased permeate flux and improved rejection [4], RO

energy consumption decreased dramatically over the years, to values that nowadays are only two or three times thermodynamic minimum, making RO currently the most energy-efficient desalination method [5]. Besides production of water for human consumption and agriculture, RO technology has many different applications, such as in food processing, and use in the pharmaceutical, textile and paper industries [6].

In contrast to the immense progress in RO development over the past decades, the actual transport and separation mechanisms are not yet fully understood [7–9]. In the attempt to describe the physico-chemical processes that govern the transport and separation process in RO membranes many mathematical models were developed throughout the years. Among those models are solution-diffusion models, which assume constant pressure and concentration gradients as the only driving force in the process, pore-flow models based on the pressure difference as driving force, and molecular dynamics simulations that address the mechanism on the molecular level, thereby taking the membrane composition also into account. In addition, irreversible thermodynamics models use a phenomenological approach to describe membrane transport [6, 10, 11].

In our present work, we aim to describe the mechanisms by which ions are transported in RO membranes using a Maxwell-Stefan approach combined with information from hydrodynamic theory of particles in thin pores. We restrict our model to the polyamide toplayer of a thin-film composite (TFC) membrane and the concentration polarization layer located in front of the membrane. We will restrict our calculations to the desalination of artificial seawater. We study the effect of applied pressure and membrane charge on the composition of the permeate, such as pH and rejection of salt, and compare with literature values.

2 Theoretical background

2.1 RO membranes

RO membranes have come a long way since the start of development of RO membranes for seawater desalination in the 1960s. The first membranes were made of cellulose acetate (CA) with the most significant development achieved by Loeb and Sourirajan [12]. Their asymmetric membrane, a 200 nm CA film on top of a porous support, laid the foundation for industrial-scale seawater desalination by RO [13]. Although the CA membranes allowed for at least an order of magnitude higher water flux than common membranes available at the time, these membranes were not durable when exposed to pH changes, chlorine and microbial contamination. Since then, many types and forms of RO membranes have been developed. Today the most common RO membrane used in commercial installations around the world is a TFC membrane with a polyamide (PA) toplayer. This material was introduced in the 1970s [14] and provides a better performance than CA membranes in terms of flux, salt rejection, pH tolerance and operational temperature range [14, 15]. These membranes consist of a very thin layer of aromatic PA (0.05–0.15 μm thickness) on top of a microporous support (pores 2 nm [16], 40 μm thickness) and a fabric layer (120–150 μm thickness) which supplies mechanical strength [13, 17, 18]. The PA layer is created through on-surface polymerization of diamine and tricarboxyl monomers on the supporting structure leading to the polyamide structure. The PA layer is a (highly) crosslinked polymer, and thus one of the monomers contains at least three functional groups – two for propagation and one for crosslinking. The membrane layer can subsequently be coated with another polymer layer (e.g. polyvinyl alcohol, polyethyleneimine), for instance to supply additional protection from fouling [14, 17, 19], but this layer can also cause flux reduction [14].

Essential in the PA toplayer is obviously the presence of pores. In RO, the pores in the membrane refer to the percolated free volume that is present between the polymer chains in the PA toplayer. The number of pores and the pore size distribution depend on the polymerization process [11]. Relative to nanofiltration membranes, RO membranes have a more narrow size distribution, i.e., a more uniform pore size [20], typically in the range of an average diameter between 0.66 and 0.78 nm [20–22]. Kim *et al.* [23] distinguished between two types of pores. The smaller type, “network pores”, are defined as the gaps between polymer branches, while “aggregate pores” relate to the spaces between polymer aggregates. Network pores have a smaller size ($\sim 0.4\text{--}0.5$ nm) and constitute about 70% of the pore volume, while aggregate pores ($\sim 0.7\text{--}0.9$ nm) account for the remainder [23, 24].

The charge of TFC RO membranes is a consequence of the polymerization process. Carboxylic and amine functional groups that did not participate in the crosslinking process or in chain elongation reactions, remain free and can be protonated or deprotonated depending on pH [24]. Protonated amine groups result in positive charge and deprotonated carboxyl groups in negative charge. This means that the membrane can have a positive or negative charge which can be described as a function of pH, as will be discussed in more detail in section 3.5.

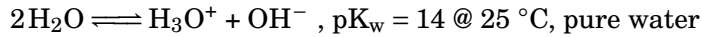
2.2 Seawater characteristics

Seawater is the largest water body available on earth – a fact that makes it an attractive, inexhaustible source for drinking water. Seawater is characterized by high salinity (“total dissolved solids” (TDS) > 35 g/L) with sodium and chloride being the major ions. pH value of seawater is slightly basic and typically is around pH 8.0. With the development and advances in RO technology throughout the years, the usage of seawater as a source of potable water rises, at present estimated at 60% of the global intake for RO desalination [25]. Table 1 presents an example of a typical seawater composition.

Table 1: Composition of mediterranean seawater for most common ions [26, 27].

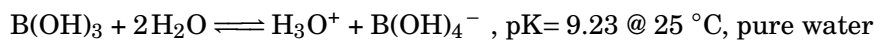
Species	Concentration (mg/L)
Na ⁺	12,500
Mg ²⁺	1,450
Ca ²⁺	450
K ⁺	450
Cl ⁻	22,100
SO ₄ ²⁻	3,410
HCO ₃ ⁻	160
B	4-5
pH	8.1

Several acid-base reactions occur in (sea)water, which must be included in the theory. In all cases we will assume that the reaction is infinitely fast, and thus, locally, the ions participating in the reaction are at chemical equilibrium with one another. First of all we must consider the auto-protolysis reaction of water, in which a proton is transferred from one molecule to the other by



The value of pK_w for pure water at 25 °C of $\text{pK}_w \sim 14$, drops to lower values for more saline solutions [28, 29].

Boron is an element present in natural water systems. Seawater contains about 5 mg/L of elementary boron [28, 30], which is predominantly in one of two forms: boric acid $\text{B}(\text{OH})_3$ and the borate ion $\text{B}(\text{OH})_4^-$. For boron concentrations higher than 22 mg/L, other species, mainly cyclic forms, may be present as well, depending on pH [31]. The distribution between boric acid and borate is given by

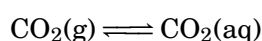


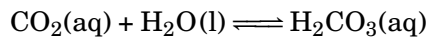
It was shown in ref. [31] that salinity affects pK , bringing it down to $\text{pK} = 8.60$ for 40 g/L TDS.

The degree of rejection of boron in seawater RO is of considerable concern. In low concentrations it has been shown that boron is beneficial to human health such as for cell metabolism, bone density and immune response [32, 33], as well as being essential to proper growth of plants. It participates in cell distribution, growth and metabolism, respiration regulation and photosynthesis. Documented cases of high boron intake occasionally reported abdominal pain, vomiting and diarrhea. In some cases fever, rash and muscle cramps were documented [34, 35]. Based on these and other findings regarding boron toxicity, and because of the incomplete understanding of the influence of boron on human health, the World Health Organization (WHO) originally recommended a guideline of a maximum concentration of 0.5 mg/L total boron in drinking water [36]. Since 2009 the guideline recommended by the WHO is set at 2.4 mg/L [37] (2.0 mg/L according to ref. [38]). According to WHO, this value can be challenging to achieve, depending on the water source and the used treatment technology [37]. Though this limit seems sufficiently low for safe human consumption of potable water, this concentration is too high when the water is used for irrigation purposes, and lower boron concentrations must be reached, depending on crop type [39].

In desalination by RO, it is argued that boron in the acid (hydrated) form passes through the RO membrane quite freely while the borate ion is rejected. The borate ion is weakly hydrated and thus relatively small [40] and we can assume the same holds for the boric acid molecule. Since boron rejection depends on the distribution between the uncharged and charged form, determined by the equilibrium constant, pH and temperature are expected to influence boron rejection. In addition, the membrane itself can enhance borate ion rejection when it is negatively charged. To facilitate rejection, the pH of the feed has to be around 8.0 in order to achieve about 88–93% rejection [41]. To further reduce boron concentration in the effluent, RO plants must use an additional RO step, boron selective resins and/or pH adjustments, to meet regulations on boron concentration [42].

The carbonate system functions as a buffer system in natural water and is the main contributor to the ability of seawater to buffer pH changes. The seawater carbonate system is in equilibrium with the CO_2 in the air, which in its dissolved form becomes H_2CO_3 (carbonic acid). The equilibria in water are given by





Note that also for the carbonate system it was shown that pK is a function of salinity, resulting in $\text{pK}_{\text{H}_2\text{CO}_3} = 5.98$ and $\text{pK}_{\text{HCO}_3^-} = 9.16$ for a 30 g/L salt solution at 25 °C [43, 44]. In RO, it is known that the permeate is characterized by trace amounts of HCO_3^- and CO_3^{2-} . The rejection of carbonate by RO membranes therefore increases carbonate concentrations in the brine, which can lead to precipitation of components such as CaCO_3 and MgCO_3 on the membrane surface, a phenomenon known as “scaling.”

In our work, the above equilibria are combined with the relevant transport equations which are set up for each ion individually. The resulting coupled model of rejection of weak acid systems has an inherent complexity, which lies in the fact that in addition to transport, species can form and deplete due to the various chemical equilibria.

2.3 Concentration polarization

Every membrane separation process promotes the passage of some species over others. This selective permeation leads to gradients of concentrations in the unmixed boundary layer in front of the membrane. For RO, if the species is rejected by the membrane it will accumulate on the surface resulting in a higher concentration (Fig. 1a) and if the membrane favors its passage, the ion will deplete (Fig. 1b). In RO, typically the salt concentration on the membrane surface is increased, creating concentration gradients in a boundary layer between the bulk solution and the membrane surface. This phenomenon of concentration polarization (CP) is a crucial parameter in RO systems because it leads to a larger salt concentration difference across the membrane and an increase in the osmotic pressure of the solution on the surface of the membrane. In addition, it promotes scaling and “cake layer” development on the membrane surface. These combined effects eventually result in a reduction of performance of the RO system.

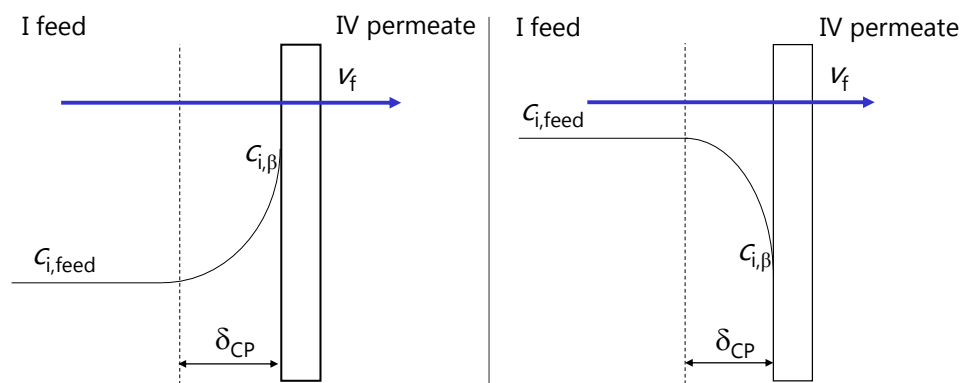


Figure 1: Sketch of concentration polarization in reverse osmosis for the case where (a) a component is enriched at the membrane surface and (b) when a component is depleted. Situation (a) is the typical situation in RO when ionic species are rejected by the membrane, but for some species the opposite behavior is possible.

3 Model equations

To model ion rejection and water recovery by RO membranes, appropriate transport models must be set up. Traditionally, there have been two important mechanistic models to describe membrane transport processes: The solution-diffusion (SD) model and the fine capillary pore (FCP) model [45]. In the SD model the three transport steps of adsorption, diffusion and desorption are each considered. The case of separating water from dissolved salts results in simplified transport equations due to additional assumptions such as constant water (solvent) concentration in the membrane and equal total pressure on the boundary between membrane and feed side. The SD model provides two membrane parameters which can be determined experimentally, and thus the SD approach offers a method to estimate and plan an RO process. Yet this model simplifies the actual transport mechanisms extensively and does not describe the complexity of the system and acting forces in detail. Instead, the FCP model approaches the film layer as a porous layer with pores of a certain size through which the hydrated ions move. The support layer can also be described in this way, only with much larger pores, but is usually neglected in the theory.

A general description of our modeling framework is presented in Figure 2. Like in the FCP model, in the present work we describe the active layer (III) as a porous material with tortuous pores of a uniform pore size which is of the same order (but larger than) the size of the solutes, thus hindering ion movement. Transport is being described with a Maxwell-Stefan approach, considering three contributions to ion transport: concentration gradients (diffusion), potential gradients (electromigration), and advection of ions with the flow of water. For uncharged species, such as boric acid and carbonic acid, there is no migration term involved and their transport is governed by diffusion and advection only. We will neglect friction between solutes, but for all ions include their friction with the fluid (the “free” water) as well as with the membrane. Steric partitioning and Donnan effect are included at both membrane-feed interfaces (β, γ). The phenomenon of concentration polarization in a layer in front of the membrane is included on the membrane-feed side (II).

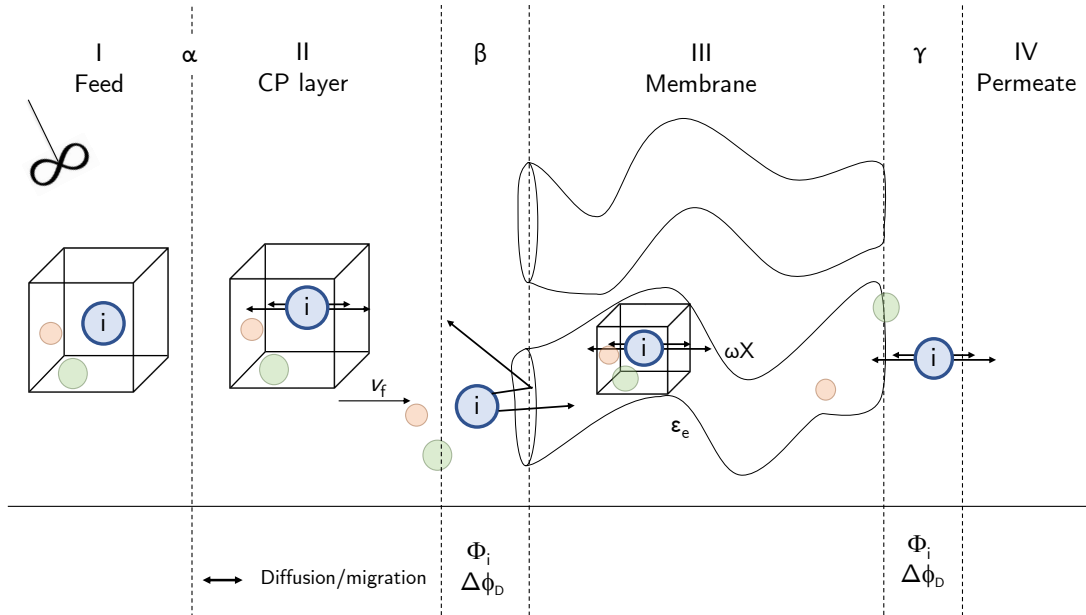


Figure 2: Description of the reverse osmosis model used in this work. α , β and γ represent the three boundaries in the system: feed-CP layer, CP layer-membrane and membrane-permeate.

3.1 Ion and molecular flux

We aim to describe the simultaneous flow of the components in the water matrix through a realistic membrane with a certain porosity and tortuosity of the pores. The derivation start with a description of a single pore, one which not necessarily follows the shortest distance across the membrane (the “direct direction”), but instead follows a path that is longer by a factor of τ . Inside such a pore, Maxwell-Stefan theory results in a relationship between the driving forces acting on an ion, and the frictions that it encounters, given by

$$-\nabla\mu_i = R_g T \sum_j \zeta_{i-j} (v'_i - v'_j) \quad (1)$$

where ζ_{i-j} is the friction factor between species i and j , R_g is the gas constant, T temperature and v'_i and v'_j are the velocities of the ions in the pore, following the path of the pore. We neglect friction between different ionic species, and only consider friction of ions with the membrane (m) and with the “free” water in between the hydrated ions (which has velocity v_f , where subscript “f” is for fluid). In that case, Eq. (1) can be written in the x' -direction as

$$-\frac{1}{R_g T} \frac{\partial\mu_i}{\partial x'} = \zeta_{i-m} (v'_i - v'_m) + \zeta_{i-f} (v'_i - v'_f) \quad (2)$$

where, since the membrane is static, we have $v'_m = 0$. We will assume ideal thermodynamic behavior for the molecules, (i.e., neglect volumetric interactions, discussed in ref. [46]) and thus the electrochemical potential, μ_i , is given by

$$\mu_i = \mu_{i,0} + R_g T (\ln c_i + z_i \phi) \quad (3)$$

where c_i and z_i are the concentration and valency of species i , and ϕ is the dimensionless electric potential. We can insert Eq. (3) in Eq. (2) which results after rearrangement in

$$v'_i = \left(\frac{\zeta_{i-f}}{\zeta_{i-f} + \zeta_{i-m}} \right) v'_f - \frac{1}{\zeta_{i-f} + \zeta_{i-m}} \left(\frac{\partial \ln c_i}{\partial x'} + z_i \frac{\partial \phi}{\partial x'} \right). \quad (4)$$

Eq. (4) shows structural similarity to hydrodynamic theory for the hindered transport of spherical particles in a pore of comparable size [47]. Utilizing this similarity, Eq. (4) can be written as [48]

$$v'_i = K_{c,i} v'_f - K_{d,i} D_{\infty,i} \left(\frac{\partial \ln c_i}{\partial x'} + z_i \frac{\partial \phi}{\partial x'} \right) \quad (5)$$

where $K_{c,i}$ and $K_{d,i}$ are called hindrance factors for convection and diffusion. These factors are only a function of the ratio between the diameter of the ion and the pore [47, 49]. Comparing Eqs. (4) with (5) shows that

$$\zeta_{i-f} = \frac{K_{c,i}}{K_{d,i} D_{\infty,i}}. \quad (6)$$

Note that up to now we have only considered transport within a pore. However, we need to develop a model for fluxes in an actual membrane where part of the structure is not accessible to the ions and water, and in addition, where the paths of the pores are not straight but tortuous (i.e., longer than the shortest direction across the membrane). To account for this, we first implement $dx' = \tau dx$, with τ tortuosity, where x is the coordinate following the shortest distance across the membrane (“direct direction”), and x' is a coordinate along the actual path in the tortuous pore. This modification corrects for the fact that in a pore that is at an angle to the direct direction across the membrane, the average driving force is lower. Furthermore, velocities v' used above

are defined along the direction of the tortuous pore, and relate to a superficial velocity v (per unit total membrane area, in the direct direction) by $v = v'\epsilon/\tau$ where ϵ is membrane porosity. Inserting these relations between x' and x , and between v' and v , leads to

$$v_i = K_{c,i}v_f - K_{d,i}\epsilon_e D_{\infty,i} \left(\frac{\partial \ln c_i}{\partial x} + z_i \frac{\partial \phi}{\partial x} \right) \quad (7)$$

where $\epsilon_e = \epsilon/\tau^2$, and multiplying Eq. (7) with c_i results for the flux of ion type i in

$$J_i = K_{c,i}c_i v_f - K_{d,i}\epsilon_e D_{\infty,i} \left(\frac{\partial c_i}{\partial x} + z_i c_i \frac{\partial \phi}{\partial x} \right). \quad (8)$$

3.2 Water flow

Also for the the water (fluid) in the pore, we must set up a Maxwell-Stefan-based expression relating fluid velocity v_f to velocities of ions and driving forces acting on the water. For the water, the required expression is closely related to Eq. (1), which in the above section was used to describe the flux of ions. Eq. (1) is a force balance on one ion (one mole of ions) which has friction with the water (filling all space between the ions), pore walls and other ions. For water, we set up a balance per pore volume, V , thus the left-hand side of Eq. (1) becomes $-\nabla \mu_w c_w (1 - \eta) V$ where c_w is the concentration of water (in water) which is given by $c_w = 1/V_w$ where V_w is the molar volume of a water molecule, and where η is the volume fraction of all (hydrated) ions in the pore (i.e., the volume excluded for “free” water), which we set to zero from this point onward.

For the friction exerted on the water that is in a volume V , we start with the expression on the right-hand side of Eq. (1), multiplied again by V and for the water-ion frictions multiplied by the concentration of ions, not of the water. This can be understood from the fact that the right-hand side of Eq. (1) describes the friction of one ion (or one mole of ions) with the continuum phase of water (and pore walls, and other ions), but we are now interested in the friction of all water that is in a volume V with all ions present in that volume. Next, we implement in the resulting equation that for water the chemical potential is given by

$$\nabla \mu_w = V_w R_g T \nabla P^t \quad (9)$$

where the total pressure P^t is given by [51]

$$P^t = P^h - \Pi \quad (10)$$

where P^h and Π are the hydraulic and osmotic pressure, both in units of mol/m³ (meaning, pressure in Pa, divided by $R_g T$). For ideal molecules, i.e., without volume effects, the osmotic pressure is a summation of species concentrations (excluding water molecules), multiplied by $R_g T$, $\Pi = R_g T \sum_i c_i$ [50–52]. Finally, we include a term for friction between water and pore walls, and then arrive at [50]

$$\frac{\partial P^t}{\partial x'} = -f'_{f-m} v'_f + \sum_i \zeta_{i-f} c_i (v'_i - v'_f) \quad (11)$$

where the first term relates to the friction of water (fluid) with the pore walls, and the summation on the right-hand side runs over all ions (not water). The parameter f'_{f-m} is the fluid-membrane friction coefficient (defined for the pore) in units of mol·s/m⁵.

In the above derivations for transport of ions and free water in the pore, we have assumed that the ions occupy no volume. This assumption is (implicitly) made at various points, e.g., when we equate velocity v'_f in Eq. (2) with that in Eq. (5), and when we neglect the effect of ion volume

in Eq. (3) and in the derivation of Eq. (11). One question is at which points in the derivation we must use for the fluid velocity the interstitial fluid velocity, i.e., the actual velocity of the free water in the space left open by the ions, and where a superficial (but still pore based) velocity is required. In future work, the volume occupied by ions in the pore should be included in more detail in the transport equations, describing how it affects the force balance for water, and the recalculation of v_f , but in the present work we assume in the transport part of the model that the ion volume fraction is set to $\eta = 0$ (ion volume does play a role in the calculation of partition coefficients and hydrodynamic hindrance functions).

Inserting Eqs. (5) and (6) in Eq. (11), and making the conversions from x' to x and v' to v , results in

$$-\frac{\partial P^t}{\partial x} = \frac{1}{\epsilon_e} \left(f'_{f-m} + \sum_i c_i \zeta_{i-f} (1 - K_{c,i}) \right) v_f + K_{c,i} \left(\frac{\partial}{\partial x} \sum_i c_i - \omega X \frac{\partial \phi}{\partial x} \right) \quad (12)$$

where we implemented the local electroneutrality condition in the membrane

$$\sum_i z_i c_i + \omega X = 0 \quad (13)$$

where ωX is the membrane charge density, to be discussed in detail in the next section. By setting $K_{c,i} = 1$ (i.e., no ion-wall friction), Eq. (12) results in the classical expression [53]

$$\frac{\partial P^h}{\partial x} + f_{f-m} v_f = \omega X \frac{\partial \phi}{\partial x} \quad (14)$$

where $f_{f-m} = f'_{f-m} / \epsilon_e$.

In the following sections we describe further elements of the model, relating to the PA toplayer in the membrane, pore and ion sizes, partitioning at membrane edges, hindrance factors and membrane charge.

3.3 Effective ion and pore sizes in PA membrane

For the TFC SWRO membrane that we model, it was assumed that the main resistance to transport in the membrane derives from the polyamide layer and therefore the membrane description is of that layer alone. The layer was considered to be a rigid structure [11, 20, 54] and thus we chose a defined pore size. An average pore size of 0.76 nm [20, 55] and film thickness of 100 nm were assumed. These values are within the range of values reported in literature [11, 18, 20, 22, 24, 55, 56]. Owing to the aqueous environment in the membrane, species were described with their solvation shell included. However, since the hydrated size of carbonate and bicarbonate exceeds the value for pore size assumed, it was considered that they have to, at least partially, shed their solvation shell, and thus for the carbonate species radii were chosen to represent partially hydrated ions yielding $\lambda_i < 1$. All ion sizes used in the model are summarized in Table 2.

3.4 Donnan-steric partitioning

As a result of membrane charge, an electrochemical potential develops on both membrane edges (at the bulk–membrane interfaces, β and γ , see Fig. 2). This phenomenon is known as the Gibbs-Donnan effect and the electric potential difference as Donnan potential. Based on the calculated value of the Donnan potential we can relate the concentration of the ions between both sides of the boundary. It has been suggested that for the ions to be able to enter the pores they have to,

at least partially, loose or rearrange their solvation shell which in turn poses an energy barrier for the process [24,57]. However, in the present work, we only account for the steric disturbance, by introducing a partitioning coefficient at the membrane-solution interface, described by

$$\Phi_i = (1 - \lambda_i)^2 \quad (15)$$

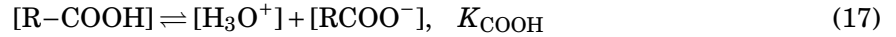
where λ is the ratio between the ion size and the pore size. Combining the partitioning and electrostatic effects, we obtain

$$c_{i,m} = c_{i,\infty} \Phi_i \exp(-z_i \Delta\phi_D) \quad (16)$$

where $\Delta\phi_D$ is the dimensionless Donnan potential (Donnan potential divided by $R_g T/F$) and subscript m refers to a point just within the membrane, and ∞ to just on the outside.

3.5 Membrane charge

Coronell *et al.* quantified the charged functional groups in an FT30 RO membrane [24]. They found that while ionized amine groups can be described by one dissociation constant, pK_{NH_2} , two values were required to adequately describe the carboxylic groups, pK_{COOH_1} , pK_{COOH_2} . The equilibrium for the carboxylic groups is given by



where $R-$ represents the polymer backbone. Note that throughout this work, all K and pK -values for chemical equilibria refer to acid constants. Utilizing the relation between concentration and equilibrium constant, K_{COOH} , we can write

$$[RCOOH] = \frac{[H_3O^+][RCOO^-]}{K_{COOH}} \quad (18)$$

and due to the fixed number of carboxylic groups, at all times

$$[RCOOH]_{tot} = [RCOO^-] + [RCOOH] \quad (19)$$

and with $X_{COOH} = [RCOOH]_{tot}$, we arrive at

$$[RCOO^-] = X_{COOH} / \left(1 + \frac{[H_3O^+]}{K_{COOH}} \right). \quad (20)$$

Similarly, for the amine surface groups, equilibrium is given by



and considering conservation of amine groups, the expression for the protonated amine group is

$$[RNH_3^+] = X_{NH_2} / \left(1 + \frac{K_{NH_2}}{[H_3O^+]} \right). \quad (22)$$

Assuming fast equilibrium and taking into account both carboxylic groups, we use Eqs. (20) and (22) to write

$$\omega X = X_{NH_2} / \left(1 + \frac{K_{NH_2}}{[H_3O^+]} \right) - X_{COOH_1} / \left(1 + \frac{[H_3O^+]}{K_{COOH_1}} \right) - X_{COOH_2} / \left(1 + \frac{[H_3O^+]}{K_{COOH_2}} \right) \quad (23)$$

which describes the membrane charge at any given H_3O^+ concentration in the PA layer, i.e. for any local pH. The result of Eq. (23) is plotted as function of pH in Fig. 3, based on data/input of

ref. [24]. Though the membrane charge as measured in ref. [24] is determined as a concentration per unit total volume of the toplayer, in the present work we use their result as if it is the membrane charge per unit pore volume.

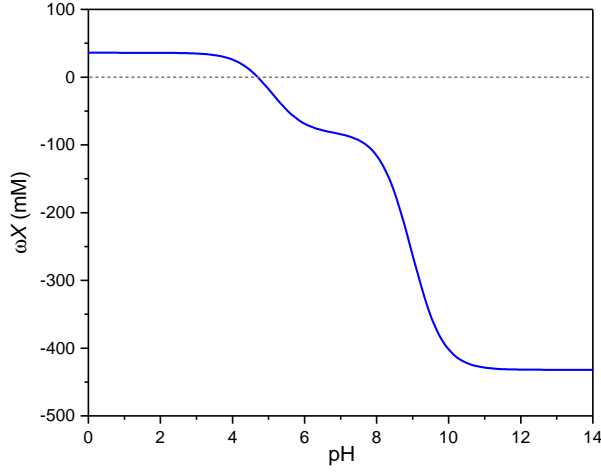


Figure 3: Fixed membrane charge in polyamide RO membrane toplayer, as a function of local pH. Calculated from ref. [24].

3.6 Hindered transport

Since the pore molecular size is not much larger than that of the ions, it is important to include the pore size in the transport model. Here we rely on hindered transport theory, as developed and discussed in literature [47, 49]. The expressions for the steric hindrance coefficients divide into two ranges. For $0 < \lambda_i < 0.8$ the expression was adapted from Bowen *et al.* [58] and for $0.8 < \lambda_i < 1$ from Bandini and Vezzani [59], which are given by

$$\begin{aligned}
 K_{c,i} &= \begin{cases} 1.0 + 0.054\lambda_i - 0.988\lambda_i^2 + 0.441\lambda_i^3 & 0 < \lambda_i < 0.8 \\ -6.83 + 19.348\lambda_i - 12.518\lambda_i^2 & 0.8 < \lambda_i < 1 \end{cases} \\
 K_{d,i} &= \begin{cases} 1.0 - 2.30\lambda_i + 1.154\lambda_i^2 + 0.224\lambda_i^3 & 0 < \lambda_i < 0.8 \\ -0.105 + 0.318\lambda_i - 0.213\lambda_i^2 & 0.8 < \lambda_i < 1 \end{cases}
 \end{aligned} \tag{24}$$

The values for λ_i , $K_{c,i}$ and $K_{d,i}$ used in the model are presented in Table 2.

3.7 Concentration polarization (CP) layer

For the description of the CP layer in front of the membrane, the same transport equations were used as presented above, but now excluding hindered transport, as well as porosity and tortuosity effects, and thus ionic flux in the CP layer is described by the Nernst-Planck equation,

$$J_i = c_i v_f - D_{\infty,i} \left(\frac{\partial c_i}{\partial x} + z_i c_i \frac{\partial \phi}{\partial x} \right) \tag{25}$$

while Eq. (14) results in the fact that in the CP-layer the hydrostatic pressure gradient is zero. The model considers a CP layer thickness of $\delta_{CP} = 20 \mu\text{m}$ [3]. Electroneutrality in the CP layer is given by Eq. (13) with $\omega X = 0$.

3.8 Auxiliary relations for ionic fluxes

Several additional relations are required to obtain a complete model. First of all, in RO the ionic current, J_{ch} , is zero, and thus the summation of all ion fluxes (times valency) must be zero at each point in the CP layer, as well as at each point in the membrane. Thus, at each point

$$J_{\text{ch}} = \sum_i z_i J_i = 0. \quad (26)$$

Until now we have not yet explicitly described how the acid/base reactions play a role in the structure of the model. As mentioned in section 2.2, transport of weak acid systems, such as boric and carbonic acid, is more complex to describe because of the local chemical equilibrium that is affecting concentrations. This is in contrast to strong acid systems where the equilibrium constant is large enough to neglect changes that occur due to a disturbance of chemical equilibrium. In our model, we take into consideration that all species, except for sodium and chloride, relate to each other through a reaction involving the hydronium ion. This means that a change in the concentration of for instance HCO_3^- , will actuate a change in concentration of H_2CO_3 and HCO_3^- and of H_3O^+ , OH^- , but also of $\text{B}(\text{OH})_3$ and $\text{B}(\text{OH})_4^-$. What this implies is that in the mathematical code, because we work at steady-state, the flux not of an individual ion, like HCO_3^- , is invariant across the membrane (and the same at any point in the CP layer), but only the flux of the *group* of the three carbonate species together [60]. And the same holds for the group of the two boron species. Note that it is not necessary to set up a flux equation for H_3O^+ and OH^- [60]. The diffusion coefficient of these species only shows up in the expression for the ionic current, Eq. (26).

Finally, we need to relate the concentration in the permeate to the fluxes through the membrane. For the dead-end cell experiments we consider, the following relationship then holds, where

$$c_{i,\text{permeate}} = J_i/v_f. \quad (27)$$

It is important to note that in this form, Eq. (27) can only be used for Na^+ and Cl^- . For the carbonate and borate groups, Eq. (27) is used for the flux and concentration of the entire group. Eq. (27) should not be used for H_3O^+ and OH^- .

All equations are discretized and solved in steady-state, for a given feed composition, and given fluid flow rate, v_f . The hydrostatic pressure difference, ΔP^h , required to achieve a given flow rate, is calculated afterwards.

4 Results and Discussion

4.1 Input parameters in the model

In this section we will present results of calculations for one given feed seawater composition, and one set of input parameters for ion size, diffusion coefficients, etc. The only parameters that will be changed are the water flow rate through the membrane, v_f , membrane charge, and seawater feed pH. All input parameters used in the model are listed in Table 2. Note that in this section (and throughout this paper), the words “membrane” and “PA toplayer” are both used, and have the same meaning. The same goes for the words (“free”) water and “fluid”.

Table 2: Inputs used in the simulation.

* Based on Stokes-Einstein relation using $\mu_w = 8.9 \cdot 10^{-4}$ Pa.s [61].

† Partial loss of hydration shell was assumed.

‡ based on $f_{f-m} = (A\delta_m R_g T)^{-1}$ [50], with $A = 3.0 \mu\text{m}/\text{bar}/\text{s}$ [18].

	Parameter	Value	Parameter	Value
constituents	$\text{Na}^+_{\text{feed}}$	553 mM	$\text{pK}_{\text{COOH}_1}$	5.23 [24]
	$\text{Cl}^-_{\text{feed}}$	550 mM	$\text{pK}_{\text{COOH}_2}$	8.97 [24]
	$\text{B}_{\text{tot}}_{\text{feed}}$	0.5 mM [27, 62]	pK_{NH_3}	4.74 [24]
	$\text{C}_{\text{tot}}_{\text{feed}}$	2.48 mM [26, 63]	$\text{pK}_{\text{B}(\text{OH})_3}$	8.60 [44]
	pH_{feed}	8.0 [26, 27]	$\text{pK}_{\text{H}_2\text{CO}_3}$	5.98 [28]
			$\text{pK}_{\text{HCO}_3^-}$	9.16 [28]
		pK_w	13.3 [28]	
properties	d_{Na^+}	7.16 Å [64]	d_{Cl^-}	6.64 Å [64]
	$d_{\text{H}_3\text{O}^+}$	5.64 Å [64]	d_{OH^-}	6.00 Å [64]
	$d_{\text{B}(\text{OH})_3}$	3.84 Å*	$d_{\text{B}(\text{OH})_4^-}$	5.22 Å [40]
	$d_{\text{H}_2\text{CO}_3}$	3.64 Å*	$d_{\text{HCO}_3^-}$	7.16 Å†
	$d_{\text{CO}_3^{2-}}$	7.30 Å†	d_{pore}	7.60 Å [20, 55]
	$D_{\text{H}_3\text{O}^+}$	8.24×10^{-9} m ² /s [19]	D_{OH^-}	4.51×10^{-9} m ² /s [19]
	D_{Na^+}	1.33×10^{-9} m ² /s [65]	D_{Cl^-}	2.00×10^{-9} m ² /s [65]
	$D_{\text{B}(\text{OH})_3}$	1.28×10^{-9} m ² /s [61]	$D_{\text{B}(\text{OH})_4^-}$	1.18×10^{-9} m ² /s
	$D_{\text{H}_2\text{CO}_3}$	1.92×10^{-9} m ² /s [60]	$D_{\text{HCO}_3^-}$	1.18×10^{-9} m ² /s [60]
	$D_{\text{CO}_3^{2-}}$	9.8×10^{-10} m ² /s [60]		
membrane	δ_m	100 nm [18, 24, 55]	δ_{CP}	20 μm [3]
	ϵ_e	0.05 [55]	f_{f-m}	1.3×10^{14} mol/s/m ⁵ ‡
	X_{COOH_1}	82 mM [24]	X_{COOH_2}	350 mM [24]
	X_{NH_3}	36 mM [24]		
partitioning (calculated)	λ_{Na^+}	0.942	λ_{Cl^-}	0.874
	$\lambda_{\text{H}_3\text{O}^+}$	0.742	λ_{OH^-}	0.790
	$\lambda_{\text{B}(\text{OH})_3}$	0.505	$\lambda_{\text{B}(\text{OH})_4^-}$	0.687
	$\lambda_{\text{H}_2\text{CO}_3}$	0.479	$\lambda_{\text{HCO}_3^-}$	0.942
	$\lambda_{\text{CO}_3^{2-}}$	0.961		
	Φ_{Na^+}	0.00335	Φ_{Cl^-}	0.0156
	$\Phi_{\text{H}_3\text{O}^+}$	0.0665	Φ_{OH^-}	0.0443
	$\Phi_{\text{B}(\text{OH})_3}$	0.245	$\Phi_{\text{B}(\text{OH})_4^-}$	0.0981
	$\Phi_{\text{H}_2\text{CO}_3}$	0.272	$\Phi_{\text{HCO}_3^-}$	0.00335
	$\Phi_{\text{CO}_3^{2-}}$	0.00156		
hindrance (calculated)	K_{c,Na^+}	0.287	K_{d,Na^+}	0.00554
	K_{c,Cl^-}	0.519	K_{d,Cl^-}	0.0102
	$K_{c,\text{H}_3\text{O}^+}$	0.676	$K_{d,\text{H}_3\text{O}^+}$	0.0202
	K_{c,OH^-}	0.644	K_{d,OH^-}	0.0137
	$K_{c,\text{B}(\text{OH})_3}$	0.832	$K_{d,\text{B}(\text{OH})_3}$	0.161
	$K_{c,\text{B}(\text{OH})_4^-}$	0.714	$K_{d,\text{B}(\text{OH})_4^-}$	0.0373
	$K_{c,\text{H}_2\text{CO}_3}$	0.848	$K_{d,\text{H}_2\text{CO}_3}$	0.188
	K_{c,HCO_3^-}	0.287	K_{d,HCO_3^-}	0.00554
	$K_{c,\text{CO}_3^{2-}}$	0.205	$K_{d,\text{CO}_3^{2-}}$	0.00393
	R_g	8.3144 J/K/mol		
	F	96845 C/mol		
	T	25 °C		

4.2 Results as function of permeate flow rate

Before investigating the influence of water flow rate, we first present results of calculations using a permeate flow rate (water flow rate through the membrane) of $v_f = 10 \mu\text{m/s}$, which is a typical value in SWRO, and which recalculates to $36 \text{ L/m}^2/\text{hr}$ [3]. The performance of the membrane at this condition in terms of rejection of salt and boron is summarized in Table 3 and compared with values from literature. As shown in Table 3, we obtain a near-perfect match for all three properties. The model gives a slightly optimistic prediction of salt and boron rejection which suggests that in the calculation the pore size must perhaps be increased slightly. The calculated $\text{pH}_{\text{permeate}}$ is within the range of experimental data reported in ref. [66]. An elevation in $\text{pH}_{\text{permeate}}$ comparing with pH_{feed} was also observed in ref. [67] with a feed (seawater) pH of 9.0 resulting in permeate pH of 9.1–9.5. According to Eq. (12), for this water flow rate, the required applied pressure was calculated to be $\Delta P^h = 35.6 \text{ bar}$. Based on this value and the osmotic pressure of the feed solution, the thermodynamic efficiency of this process can be calculated as $\eta = 77\%$ based on $\eta = \Delta\Pi/\Delta P^h$ where the osmotic pressure difference is that across the membrane. Note that this relation is only valid for a very low water recovery and a very dilute permeate, see Eq. (3) in ref. [68].

Table 3: Summary of model output compared with values for sea water reverse osmosis reported in literature.

Parameter	Our model	Literature	Reference
$\text{pH}_{\text{permeate}}$	8.8	8.6-8.8	[66]
R_{NaCl}	99.9 %	96.6-99.8 %	[69]
R_{B}	93.5 %	87-93 %	[69]

Calculation results show that the CP layer increases the salt concentration directly on the membrane surface from $c_{\text{salt,feed}} = 550 \text{ mM}$ in the feed, to about $c_{\text{salt},\beta} = 620 \text{ mM}$. This is about a 10% increase, which is less than a typical value in RO of around 30% [3]. Thus, in our calculation the CP layer increases the osmotic pressure of the salt solution directly near the membrane surface by $\sim 4 \text{ bar}$. As observed in calculations at different values of v_f , for all species but H_3O^+ , increasing v_f always results in an increase in ion concentrations at the membrane surface.

As an example, we show in Fig. 4 concentration profiles in the CP layer and in the membrane for the boric acid and the borate ion, as well as of H_3O^+ and OH^- . For H_3O^+ and OH^- , the product of their concentrations is always the same and therefore their profiles are vertical mirror images. A condition of pH 7 is reached at a point around one third into the membrane. pH decreases by about two points when we move from the very left to the very right of the PA toplayer, and pH then increases by three points when we exit the membrane. In the membrane the neutral boric acid molecule is about an order of magnitude more prevalent than the borate anion.

Next we examined the effect of fluid flow rate (through the membrane) on system performance, both for much lower and much higher flow rates than the standard situation just discussed. Salt rejection remained almost constant throughout the examined range at a value between 99.0% and 99.9%, see Fig. 5A, while boron rejection increased from 93.5% at $v_f = 10 \mu\text{m/s}$ to $R_{\text{B}} = 98.6\%$ at $v_f = 60 \mu\text{m/s}$. Lower flow rates reduced boron retention significantly. Increasing flowrate from 10 to $40 \mu\text{m/s}$, permeate pH decreased from 8.8 to ~ 8.6 after which it increases again to reach pH 9.5 at a flowrate of $100 \mu\text{m/s}$ [results not shown]. Thus, for all flow rates,

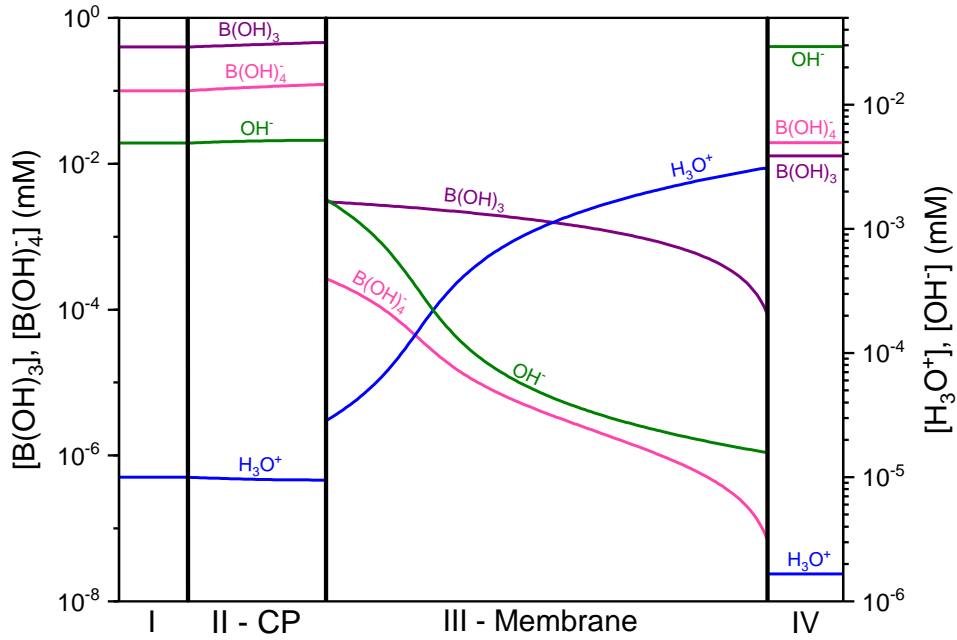


Figure 4: Concentration profiles of the two boron species and H_3O^+ and OH^- in the CP-layer (II) and membrane (III). Concentrations are plotted on a logarithmic scale. Left is the feed solution (I), right permeate (IV).

$\text{pH}_{\text{permeate}}$ was higher than feed pH .

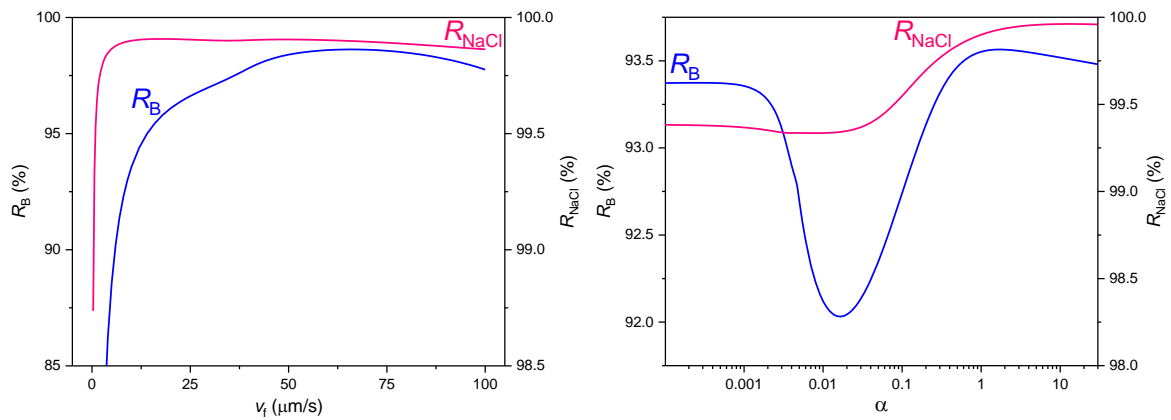


Figure 5: Rejection of NaCl and boron by the membrane as function of A) water flow rate v_f , and B) membrane charge density α , which is the factor by which the concentration of each component of membrane charge, X_k , is multiplied. Conditions of Table 2, $v_f = 10 \mu\text{m/s}$.

Figs. 6-8 show the obtained concentration profiles of the different ionic species in the membrane, for different water flow rates, v_f . Such a representation of calculation output was not found in surveyed literature and highlights the complex character of multi-component transport in membrane processes. In general, it can be seen that when v_f increases so does the ion concentration at the beginning of the membrane, except for the hydronium ion.

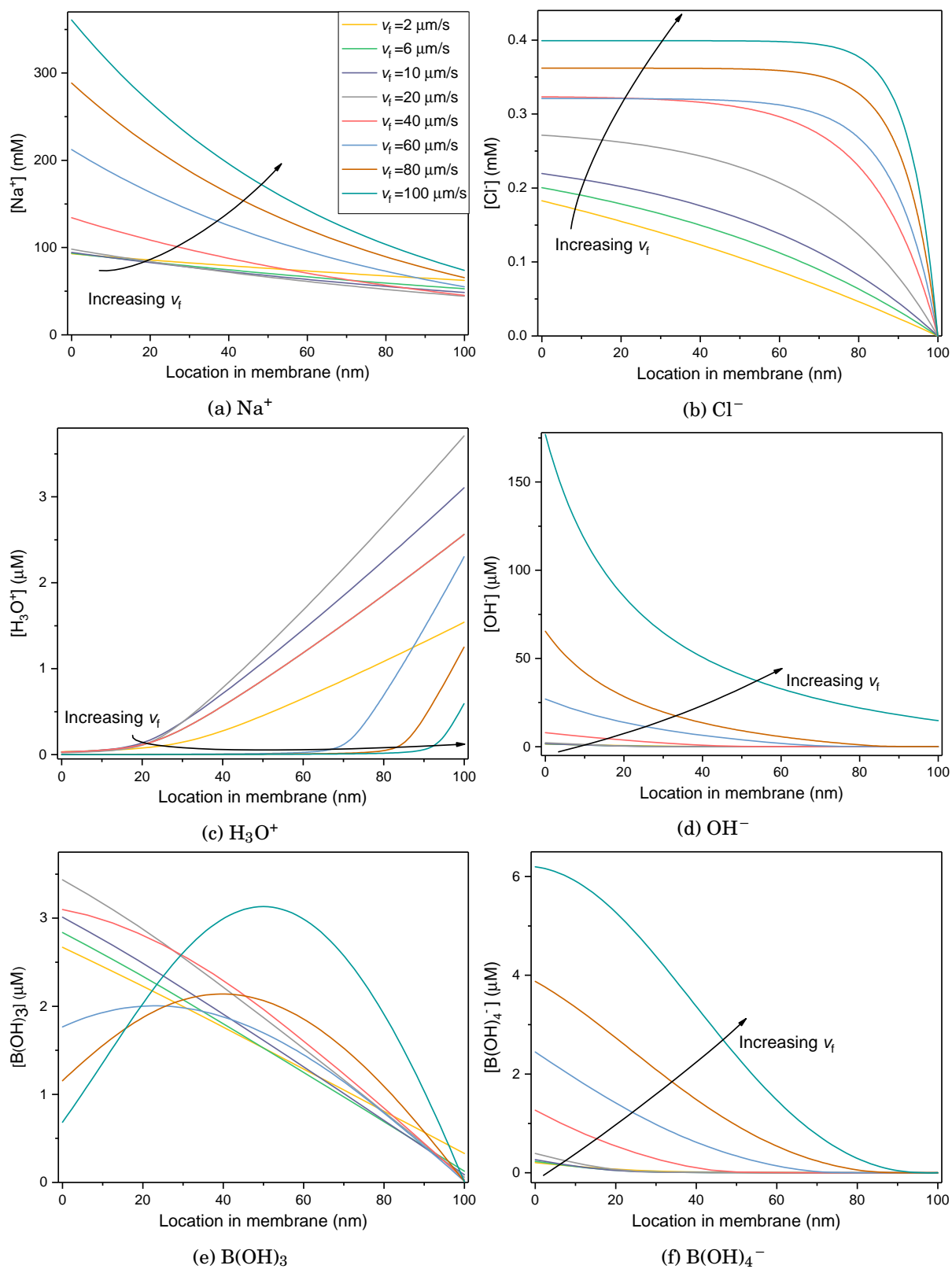


Figure 6: Concentration profiles in the membrane of Na^+ , Cl^- , H_3O^+ , OH^- , $\text{B}(\text{OH})_3$ and $\text{B}(\text{OH})_4^-$ for different values of the water flow rate v_f .

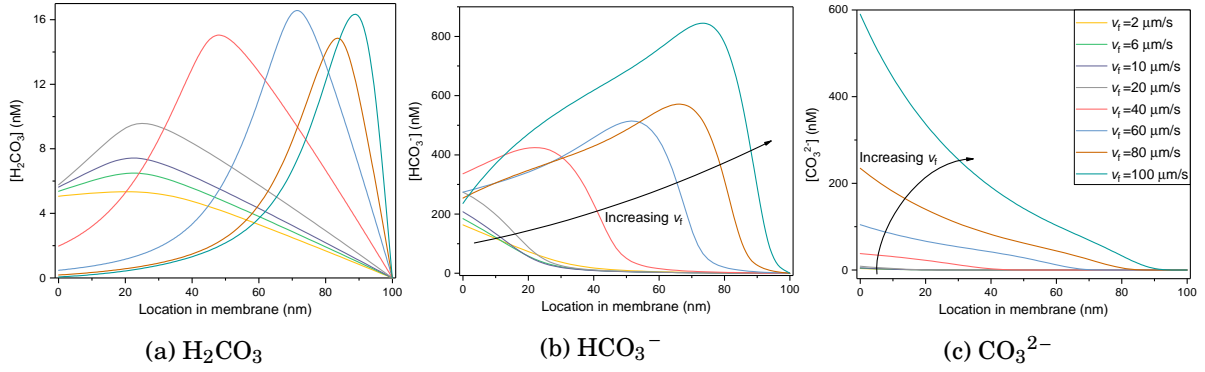


Figure 7: Concentration profiles in the membrane of H_2CO_3 , HCO_3^- and CO_3^{2-} for different values of the water flow rate v_f .

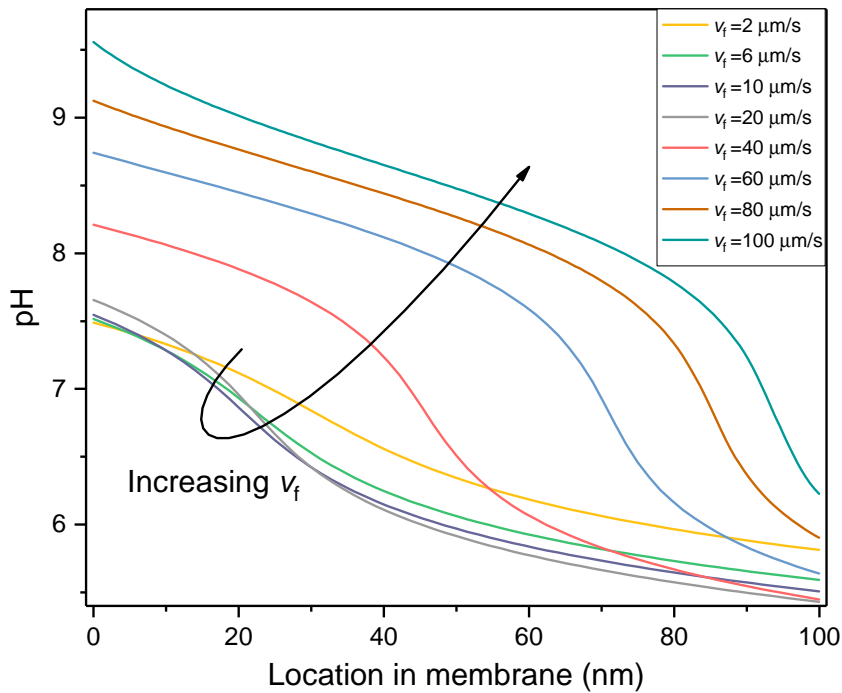


Figure 8: H_3O^+ concentration in the membrane, expressed as pH, for different values of the water flow rate v_f .

When we look at two neutral compounds, boric acid (Fig. 6) and carbonic acid (Fig. 7), we see that as v_f increases so does the concentration at the beginning of the membrane, until the trend reverses for $v_f > 20 \mu\text{m/s}$. With higher v_f , the concentration profile for boric acid becomes parabolic-like. For carbonic acid and bicarbonate, their concentration profiles become non-monotonic and a maximum concentration is found in the membrane, the location of which is being displaced deeper into the membrane layer as the water flow rate increases.

At low water flow rates ($v_f \lesssim 36 \mu\text{m/s}$) pH at the beginning of the membrane is lower than pH_{feed} . For higher water flow rates the solution becomes more basic at the beginning of the membrane, but always remains more acidic than the feed when at the other side of the membrane. At the same time, $\text{pH}_{\text{permeate}}$ was always higher than in the feed.

4.3 Sensitivity analysis

An interesting question is, what is the relative contribution of the three mechanisms that transport ions (advection, diffusion and migration) through the membrane. To analyze that question, the *magnitudes of the three terms in Eq. (7)* are separately calculated and compared. Results in Fig. 9 are based on the standard condition described in Table 2 with water flow rate $v_f = 10 \mu\text{m/s}$. We present here only diagrams for selected species. For the other species, the behavior is as follows. For Na^+ , the contribution of each mechanism is invariant across the membrane with 50% migration, 27% advection, and 23% diffusion; for OH^- , diffusion and migration are approx. the same as for H_3O^+ and advection is slightly higher; profiles for HCO_3^- and CO_3^{2-} are similar to B(OH)_4^- ; for B(OH)_3 there is no migration, and diffusion linearly increases from 90% at the entrance to 100% at the exit of the membrane.

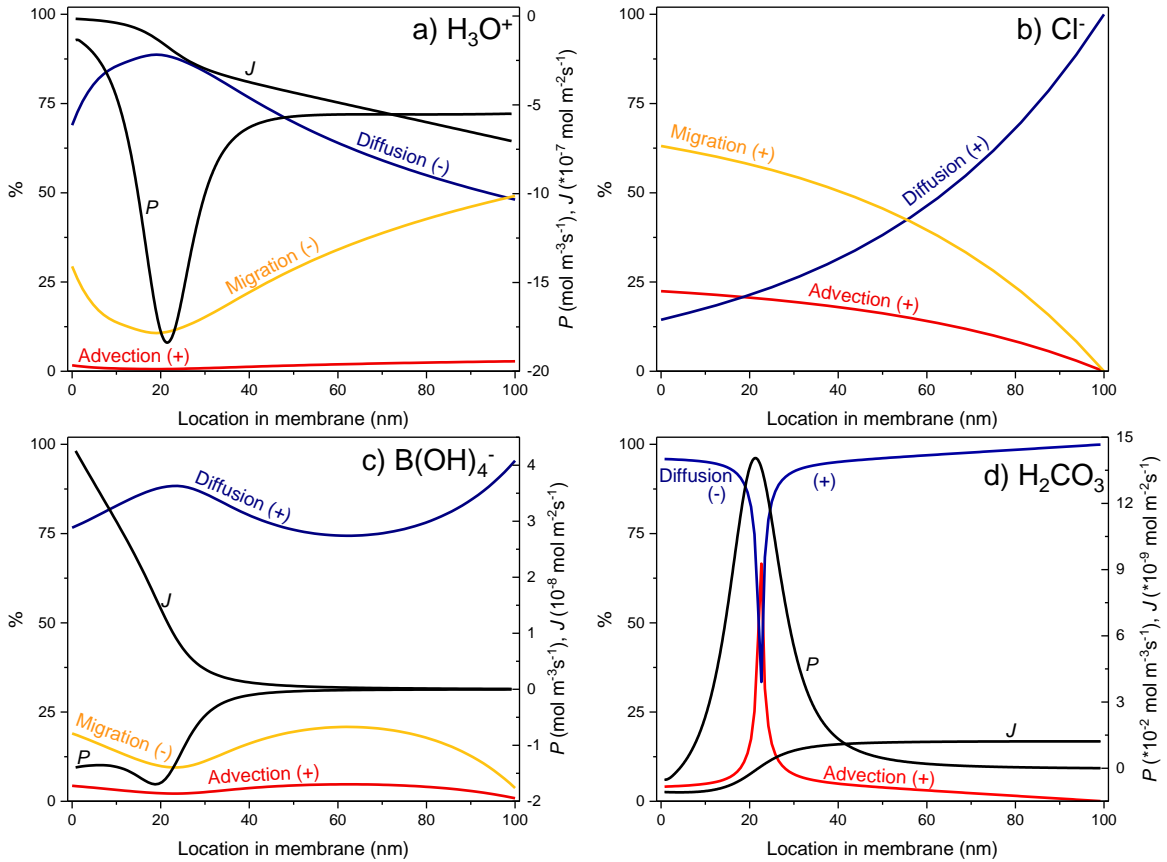


Figure 9: Relative contribution of advection, diffusion and migration to the flux of selected ions H_3O^+ , Cl^- , B(OH)_4^- and H_2CO_3 . Signs next to each line describe whether the term helps to move the ion towards the permeate (+) or towards the feed (-).

As Fig. 9 shows, the transport of all species that are present at low concentration is dominated by diffusion. This contribution of diffusion was also discussed for H_3O^+ and OH^- in ref. [9]. Other than that, the relative contribution of each term is not directly intuitive, for instance for Cl^- changing strongly across the membrane, while for carbonic acid, an extremely sharp change is observed due to the fact that at that point the diffusional contribution is zero, and only advection plays a role. Clearly the study of the relative importance of the various mechanisms driving an ion, is non-trivial and may lead to interesting insights. Furthermore, three of the four ions discussed in Fig. 9 are part of an acid/base equilibrium, and thus they can react away or be formed

within the toplayer. This implies their flux, J , changes with position, as shown in Fig. 9 because of a chemical production term, P . Because we consider steady-state, the chemical production term P is equal to the gradient in J .

4.4 Effect of membrane charge

As TFC membranes are charged, we decided to examine the behavior and performance if the membrane charge would change. The standard values of the three functional groups' concentrations, X_k , were multiplied by a certain factor α , thus keeping their relative concentrations the same. We recorded the rejection of boron (Fig. 5B) and interestingly, for the current value of the membrane charge, boron rejection is almost at a maximum, which we locate at $\alpha = 1.5$ to be $R_B = 93.6\%$. Even reducing the membrane charge dramatically, there is not much of a reduction in the ability of the membrane to reject boron with $R_B = 92\%$ at a 100 times reduced membrane charge. This can be explained by the fact that the neutral boron in the form of boric acid passes the membrane while not being affected by charge. For all values of α considered, salt rejection remains very high, at values above 99.5%.

Calculation results for different values of pH of seawater (keeping the total carbonate concentration the same) are that for a 50 \times reduced membrane charge, R_B is not affected much by pH_{feed} in the entire range studied of $4 < \text{pH}_{\text{feed}} < 10$ [not shown]. However, for the standard value of membrane charge, and one with 10 \times more charge, for pH_{feed} less than 8.0, R_B was not changed, but for pH_{feed} beyond 8, boron rejection went up significantly, up to 99% at $\text{pH}_{\text{feed}} = 10$. This latter result may not be of much practical relevance, because increasing the pH of seawater would lead to severe scaling of the system.

Finally, we present our results for the effect of pH_{feed} on $\text{pH}_{\text{permeate}}$ for three different values of the membrane charge (Fig. 10). Except for very extreme pH_{feed} , in all cases $\text{pH}_{\text{permeate}}$ is higher than pH_{feed} . For $\text{pH}_{\text{feed}} \sim 8.0$, the increase is around one pH-point, which drops further at higher pH_{feed} . For lower pH_{feed} , down to pH 4, for the membranes with the original charge or larger, the permeate pH can be higher by around 3 pH points, while for the (almost) uncharged membrane, effluent pH is not more than 1 pH point higher than that of the feed. Our calculation results can also be compared to two literature sources for experimental data. For the standard value of the membrane charge ($\alpha = 1$), measurements for SWRO are well reproduced by our calculations: for $\text{pH}_{\text{feed}} = 8.0$ we predict $\text{pH}_{\text{permeate}} = 8.7$, while experimentally a value of $\text{pH}_{\text{permeate}} = 8.6\text{--}8.8$ is reported [66], and for $\text{pH}_{\text{feed}} = 9.0$, we predict $\text{pH}_{\text{permeate}} = 9.1$ while the experimental value is $\text{pH}_{\text{permeate}} = 9.1\text{--}9.5$ [67].

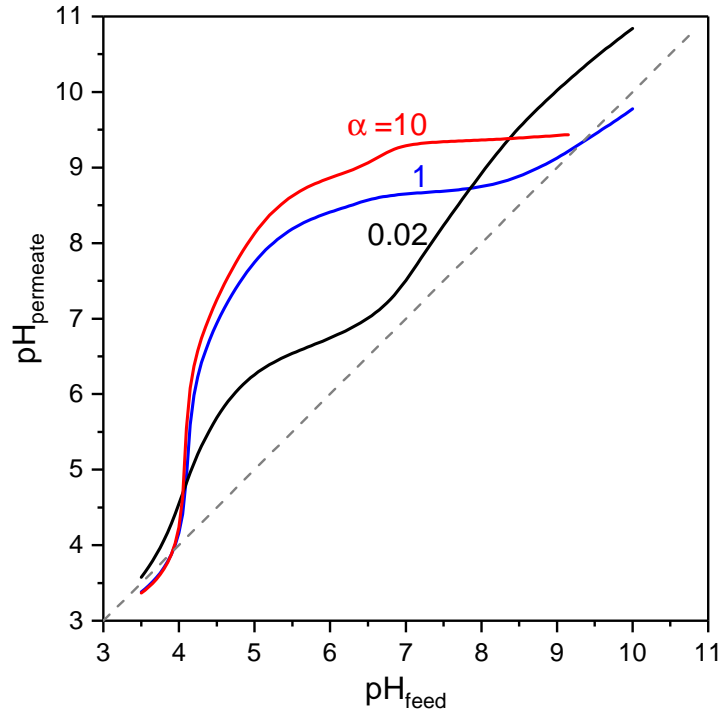


Figure 10: $\text{pH}_{\text{permeate}}$ as a function of pH_{feed} , for three different values of the relative membrane charge α , for conditions of Table 2, $v_f = 10 \mu\text{m/s}$.

5 Conclusions

In this work we have developed and applied a theoretical transport model to describe the desalination of seawater using a flat sheet TFC-SWRO membrane. The water matrix was chosen to mimic seawater composition and contains high concentrations of NaCl, which is contrary to most other studies, which model salt rejection in more dilute systems. We investigated the influence of water flowrate (pressure), membrane charge and seawater pH. The water equilibrium and two weak acid systems - boric and carbonic acid - were considered additionally to the major ionic constituents. In the model, the membrane was considered to be a tortuous-porous polymeric structure, that holds a fixed amount of pH-dependent charge. Transport in the membrane was described by a Maxwell-Stefan approach including three driving forces contributing to transport: advection, diffusion and electromigration. Molecules were considered to travel through the membrane while retaining their full hydration shell, except for carbonate and bicarbonate for which we had to assume a reduction in the hydrated size to make them fit into the pores. Species entry in the membrane was corrected for by considering the partitioning factor based on the size of ions. Hindered transport of ions in membrane pores was accounted for by hydrodynamic correction factors for diffusion and convection. Electrical potential differences across the membrane-solution interfaces, caused by the Donnan effect, were taken into consideration as well.

The model shows that in general diffusion is the dominant driving force of transport of ions in the membrane, while as the velocity of the fluid increased, ion concentration profiles become steeper. pH was, for all fluid velocities, lower in the membrane than in the feed, but on the permeate side was higher than feed pH. An increase in the membrane charge does not improve boron rejection but a lower membrane charge elevates permeate pH which might be helpful if second stage RO stage is employed for boron removal. Neither changes in pH or in membrane charge

affect the salt rejection significantly which always remained above 99%. pH of the permeate was successfully predicted by the model, which can be helpful in the planning of post treatment stages such as pH stabilization.

In order to validate the model in more detail, experimental verification of observed relations is relevant. It is important to note that the model relies on physico-chemical properties such as chemical equilibrium constants and hydrated ion sizes, for which some of those parameters are more sensitive than others to temperature changes and so will have to be adjusted for systems that differ greatly from a temperature 25 °C, which was the temperature considered in this work.

References

- [1] UN-Water Thematic Initiatives, “Coping with water scarcity: A strategic issue and priority for system-wide action,” http://www.un.org/waterforlifedecade/pdf/2006_unwater_coping_with_water_scarcity_eng.pdf, 2006.
- [2] A. A. Burbano, S. S. Adham, and W. R. Pearce, “The state of full-scale RO/NF desalination – results from a worldwide survey,” *Journal American Water Works Association*, vol. 99, pp. 116–127, 2007.
- [3] R. W. Baker, *Membrane Technology and Applications*. Wiley & Sons Ltd, 2004.
- [4] R. Larson, J. Cadotte, and R. Petersen, “The FT-30 Seawater Reverse Osmosis Membrane–Element Test Results,” *Desalination*, vol. 38, pp. 473–483, 1981.
- [5] M. Elimelech and W. A. Phillip, “The Future of Seawater Desalination: Energy, Technology, and the Environment,” *Science*, vol. 333, pp. 712–717, 2011.
- [6] L. Malaeb and G. M. Ayoub, “Reverse osmosis technology for water treatment: State of the art review,” *Desalination*, vol. 267, pp. 1–8, 2011.
- [7] H. Chmiel, X. Lefebvre, V. Mavrov, M. Noronha, and J. Palmeri, “Modeling of neutral solute and ion transport in charged nanofiltration membranes using computer simulation programs,” in *Handbook of Theoretical and Computational Nanotechnology* (M. Rieth and W. Schommers, eds.), vol. 5, ch. 109, pp. 93–214, American Scientific Publishers, 2006.
- [8] S. Bason, Y. Oren, and V. Freger, “Ion transport in the polyamide layer of RO membranes: Composite membranes and free-standing films,” *J. Membrane Sci.*, vol. 367, pp. 119–126, 2011.
- [9] O. Nir, N. F. Bishop, O. Lahav, and V. Freger, “Modeling pH variation in reverse osmosis,” *Water Research*, vol. 87, pp. 328–335, 2015.
- [10] J. G. Wijmans and R. W. Baker, “the Solution-Diffusion Model - a Review,” *Journal of Membrane Science*, vol. 107, pp. 1–21, 1995.
- [11] M. Shen, S. Keten, and R. M. Lueptow, “Dynamics of water and solute transport in polymeric reverse osmosis membranes via molecular dynamics simulations,” *Journal of Membrane Science*, vol. 506, pp. 95–108, 2016.
- [12] S. Loeb and S. Sourirajan, “Sea Water Demineralization by Means of an Osmotic Membrane,” *ACS Advances in Chemistry* **38** 117-132 (1963).

- [13] K. P. Lee, T. C. Arnot, and D. Mattia, "A review of reverse osmosis membrane materials for desalination-Development to date and future potential," *Journal of Membrane Science*, vol. 370, pp. 1–22, 2011.
- [14] D. Li and H. Wang, "Recent developments in reverse osmosis desalination membranes," *Journal of Materials Chemistry*, vol. 20, p. 4551–4566, 2010.
- [15] Lenntech, "Reducing the Fouling Rate of Surface and Waste Water RO Systems," [http://www.lenntech.com/Data-sheets/Getting the most out of your RO.pdf](http://www.lenntech.com/Data-sheets/Getting%20the%20most%20out%20of%20your%20RO.pdf), 2017.
- [16] B. D. Zdravkov, J. J. Cermák, M. Sefara, and J. Janků, "Pore classification in the characterization of porous materials: A perspective," *Central European Journal of Chemistry*, vol. 5, no. 4, pp. 1158–1158, 2007.
- [17] R. J. Petersen, "Composite reverse osmosis and nanofiltration membranes," *Journal of Membrane Science*, vol. 83, pp. 81–150, 1993.
- [18] A. K. Ghosh, B. H. Jeong, X. Huang, and E. M. V. Hoek, "Impacts of reaction and curing conditions on polyamide composite reverse osmosis membrane properties," *Journal of Membrane Science*, vol. 311, pp. 34–45, 2008.
- [19] S. H. Lee and J. C. Rasaiah, "Proton transfer and the mobilities of the H and OH ions from studies of a dissociating model for water," *J. Chem. Phys.*, vol. 135, no. 124505, 2011.
- [20] K. Košutić, D. Dolar, and B. Kunst, "On experimental parameters characterizing the reverse osmosis and nanofiltration membranes' active layer," *J. Membrane Sci.*, vol. 282, pp. 109–114, 2006.
- [21] K. Kezia, J. Lee, A. J. Hill, and S. E. Kentish, "Convective transport of boron through a brackish water reverse osmosis membrane," *J. Mem. Sci.*, vol. 445, pp. 160–169, 2013.
- [22] Y. Yoon and R. M. Lueptow, "Removal of organic contaminants by RO and NF membranes," *Journal of Membrane Science*, vol. 261, pp. 76–86, 2005.
- [23] S. Kim and E. M. V. Hoek, "Modeling concentration polarization in reverse osmosis processes," *Desalination*, vol. 186, pp. 111–128, 2005.
- [24] O. Coronell, B. J. Mariñas, X. Zhang, and D. G. Cahill, "Quantification of functional groups and modeling of their ionization behavior in the active layer of FT30 reverse osmosis membrane," *Environmental Science and Technology*, vol. 42, pp. 5260–5266, 2008.
- [25] A. Bennett, "Desalination : 50 years of progress," *Filtration & Separation*, vol. 50, pp. 32–39, 2013.
- [26] C. Fritzmann, J. Löwenberg, T. Wintgens, and T. Melin, "State-of-the-art of reverse osmosis desalination," *Desalination*, vol. 216, pp. 1–76, 2007.
- [27] The DOW Chemical Company, "Water Chemistry and Pretreatment: Feedwater Type and Analysis," Tech Manual Excerpt, 2017.
- [28] D. Dyrssen and I. Hansson, "Ionic medium effects in sea water - A comparison of acidity constants of carbonic acid and boric acid in sodium chloride and synthetic sea water," *Marine Chemistry*, vol. 1, pp. 137–149, 1973.

- [29] A. G. Dickson and J. P. Riley, "The Estimation of Acid Dissociation Constant in Seawater Media from Potentiometric Titrations with Strong base," *Marine Chemistry*, vol. 7, pp. 89–99, 1979.
- [30] R. E. Zeebe, A. Sanyal, J. D. Ortiz, and D. A. Wolf-Gladrow, "A theoretical study of the kinetics of the boric acid-borate equilibrium in seawater," *Marine Chem.*, vol. 73, pp. 113–124, 2001.
- [31] K. L. Tu, L. D. Nghiem, and A. R. Chivas, "Boron removal by reverse osmosis membranes in seawater desalination applications," *Sep. Purif. Techn.*, vol. 75, pp. 87–101, 2010.
- [32] E. Mastromatteo and F. Sullivan, "Summary: International symposium on the health effects of boron and its compounds," *Environm. Health Persp.*, vol. 102, pp. 139–141, 1994.
- [33] T. A. Devirian and S. L. Volpe, "The Physiological Effects of Dietary Boron," *Critical Reviews in Food Science and Nutrition*, vol. 43, pp. 219–231, 2003.
- [34] T. L. Litovitz, W. Klein-Schwartz, G. M. Oderda, and B. F. Schmitz, "Clinical manifestations of toxicity in a series of 784 boric acid ingestions," *American Journal of Emergency Medicine*, vol. 6, pp. 209–213, 1988.
- [35] C. H. Linden, A. H. Hall, K. W. Kulig, and B. H. Rumack, "Acute ingestions of boric acid.," *Journal of toxicology. Clinical toxicology*, vol. 24, pp. 269–79, 1986.
- [36] World Health Organization, "Guidelines for Drinking-water Quality," 3rd Ed., pp. 104–108, http://www.who.int/water_sanitation_health/dwq/fulltext.pdf, 2008.
- [37] World Health Organization, "Guidelines for Drinking-water Quality," 4th Ed., <http://www.ncbi.nlm.nih.gov/pubmed/15806952>, 2011.
- [38] S. H. Frisbie, E. J. Mitchell, and B. Sarkar, "Urgent need to reevaluate the latest World Health Organization guidelines for toxic inorganic substances in drinking water," *Environmental health*, vol. 14, no. 63, 2015.
- [39] R.S. Ayers and D.W. Westcot, "Water Quality for Agriculture," *Food and Agricultural Organization*, p. 97, 1985.
- [40] H. Corti, R. Crovetto, and R. Fernandez-Prini, "Properties of the Borate Ion in Dilute Aqueous Solutions," *J. Chem. Soc., Faraday Trans. 1*, vol. 76, pp. 2179–2186, 1980.
- [41] E. Güler, C. Kaya, N. Kabay, and M. Arda, "Boron removal from seawater: State-of-the-art review," *Desalination*, vol. 356, pp. 85–93, 2015.
- [42] N. Hilal, G. J. Kim, and C. Somerfield, "Boron removal from saline water: A comprehensive review," *Desalination*, vol. 273, pp. 23–35, 2011.
- [43] F. J. Millero, "The thermodynamics of the carbonate system in seawater," *Geochimica et Cosmochimica Acta*, vol. 43, pp. 1651–1661, 1979.
- [44] A. G. Dickson and F. J. Millero, "A comparison of the equilibrium constants for the dissociation of carbonic acid in seawater media," *Deep Sea Research Part A, Oceanographic Research Papers*, vol. 34, pp. 1733–1743, 1987.

- [45] R. Rautenbach and A. Albrecht, "Mass transport in membranes," in *Membrane processes*, Ch. 3, pp. 48–74, Wiley & Sons Ltd, 1989.
- [46] E. Spruijt and P. M. Biesheuvel, "Sedimentation dynamics and equilibrium profiles in multicomponent mixtures of colloidal particles," *J. Phys.: Condens. Matter* vol. 26, no. 075101m 2014.
- [47] W. M. Deen, "Hindered Transport of Large Molecules in Liquid-Filled Pores," *AIChE Journal*, vol. 33, pp. 1409–1425, 1987.
- [48] A. Szymczyk and P. Fievet, "Investigating transport properties of nanofiltration membranes by means of a steric, electric and dielectric exclusion model," *J. Membrane Sci.*, vol. 252, pp. 77-88, 2005.
- [49] H. Brenner and L. J. Gaydos, "The constrained Brownian movement of spherical particles in cylindrical pores of comparable radius. Models of the diffusive and convective transport of solute molecules in membranes and porous media," *J. Colloid Interface Sci.*, vol. 58, pp. 312–356, 1977.
- [50] M. Tedesco, H. V. M. Hamelers, and P. M. Biesheuvel, "Nernst-Planck transport theory for (reverse) electrodialysis: II. Effect of water transport through the membranes," *J. Membrane Sci.*, vol. 510, pp. 370–381, 2016.
- [51] P. B. Peters, R. Van Roij, M. Z. Bazant, and P. M. Biesheuvel, "Analysis of electrolyte transport through charged nanopores," *Phys. Rev. E*, vol. 93, no. 053108, 2016.
- [52] P. M. Biesheuvel, "Two-fluid model for the simultaneous flow of colloids and fluids in porous media," *J. Colloid Interface Sci.*, vol. 355, pp. 389–395, 2011.
- [53] A. A. Sonin, "Osmosis and ion transport in charged porous membranes: a macroscopic, mechanistic model," in: E. Sélégny (Ed.), *Charged Gels and Membranes I*, pp. 255–265, 1976.
- [54] V. Freger, "Swelling and Morphology of the Skin Layer of Polyamide Composite Membranes: An Atomic Force Microscopy Study," *Env. Sci. & Techn.*, vol. 38, pp. 3168–3175, 2004.
- [55] K. Kezia, J. Lee, W. Ogieglo, A. Hill, N. E. Benes, and S. E. Kentish, "The transport of hydronium and hydroxide ions through reverse osmosis membranes," *J. Membrane Sci.*, vol. 459, pp. 197–206, 2014.
- [56] X. Zhang, D. G. Cahill, O. Coronell, and B. J. Mariñas, "Partitioning of salt ions in FT30 reverse osmosis membranes," *Applied Physics Letters*, vol. 91, no. 181904, 2007.
- [57] B. Tansel, "Significance of thermodynamic and physical characteristics on permeation of ions during membrane separation: Hydrated radius, hydration free energy and viscous effects," *Separation and Purification Technology*, vol. 86, pp. 119–126, 2012.
- [58] W. R. Bowen, A. W. Mohammad, and N. Hilal, "Characterisation of nanofiltration membranes for predictive purposes - Use of salts, uncharged solutes and atomic force microscopy," *J. Membrane Sci.*, vol. 126, pp. 91–105, 1997.
- [59] S. Bandini and D. Vezzani, "Nanofiltration modeling: The role of dielectric exclusion in membrane characterization," *Chem. Eng. Sci.*, vol. 58, pp. 3303–3326, 2003.

- [60] J. E. Dykstra, P. M. Biesheuvel, H. Bruning, and A. Ter Heijne, "Theory of ion transport with fast acid-base equilibrations in bioelectrochemical systems," *Phys. Rev. E*, vol. 90, no. 013302, 2014.
- [61] E. Goli, T. Hiemstra, W. H. Van Riemsdijk, R. Rahnemaie, and M. J. Malakouti, "Diffusion of neutral and ionic species in charged membranes: Boric acid, arsenite, and water," *Analytical Chemistry*, vol. 82, pp. 8438–8445, 2010.
- [62] H. Koseoglu, N. Kabay, M. Yuksel, S. Sarp, O. Arar, and M. Kitis, "Boron removal from seawater using high rejection SWRO membranes-impact of pH, feed concentration, pressure, and cross-flow velocity," *Desalination*, vol. 227, pp. 253–263, 2008.
- [63] Lenntech, "Major ion composition of seawater," <http://www.lenntech.com/composition-seawater.htm>.
- [64] E. R. Nightingale, "Phenomenological Theory of Ion Solvation. Effective Radii of Hydrated Ions," *Journal of Physical Chemistry*, vol. 63, pp. 1381–1387, 1959.
- [65] P. Atkins and J. de Paula, *Physical chemistry*, 9th Ed., pp. 430–468, 2009.
- [66] B. Andrews, B. Davé, P. López-Serrano, S.-P. Tsai, R. Frank, M. Wilf, and E. Koutsakos, "Effective scale control for seawater RO operating with high feed water pH and temperature," *Desalination*, vol. 220, pp. 295–304, 2008.
- [67] O. Nir, E. Marvin, and O. Lahav, "Accurate and self-consistent procedure for determining pH in seawater desalination brines and its manifestation in reverse osmosis modeling," *Water Research*, vol. 64, pp. 187–195, 2014.
- [68] P. M. Biesheuvel, "Thermodynamic cycle analysis for capacitive deionization," *J. Colloid Interface Sci.*, vol. 332, pp. 258–264, 2009.
- [69] C. Dominguez-Tagle, V. J. Romero-Ternero, and A. M. Delgado-Torres, "Boron removal efficiency in small seawater Reverse Osmosis systems," *Desalination*, vol. 265, pp. 43–48, 2011.